Estimation of Iceberg Motion for Mapping by AUVs

Peter Kimball* and Stephen Rock*†
pkimball@stanford.edu, rock@stanford.edu
*Dept. of Aeronautics and Astronautics, Stanford University
496 Lomita Mall, Stanford, CA 94305
†Monterey Bay Aquarium Research Institute
7700 Sandholdt Road, Moss Landing, CA 95039

***Abstract*—Iceberg-relative navigation for Autonomous Underwater Vehicles (AUVs) will enable a new mode of data collection for studies of free-floating icebergs. Compared to current data collection methods, AUVs offer substantially expanded coverage area and continuous sampling. However, because icebergs translate and rotate through inertial space, standard vehicle navigation methods which rely on inertial sensors are unable to provide iceberg-relative position estimates. One means of obtaining iceberg-relative position estimates is to correlate incoming sonar measurements of range to the iceberg surface with an a-priori three-dimensional iceberg map. This requires the generation of a map.**

The key challenge in creating such an a-priori map is accounting for the translation and rotation of the iceberg over the duration of map data collection. Previous iceberg mapping work by the authors accounts for iceberg motion by assuming a constant velocity model. It uses loop closure (small overlapping areas of sonar data at the beginning and end of a circumnavigation) in post-processing to identify the value of the iceberg velocity. The result is a self-consistent iceberg map suitable for iceberg-relative vehicle navigation. However, the map can be somewhat warped relative to the true shape of the iceberg due to any innacuracies in the constant velocity assumption.

This paper presents an extended iceberg mapping method which uses a more complex motion model, capable of more accurately representing the motion of the iceberg and therefore of providing a more accurate iceberg map. To identify the parameters in this model, the extended method incorporates Doppler sonar measurements which give information about the velocity of the iceberg throughout the circumnavigation. Because the Doppler velocity measurements depend on the trajectory of the iceberg and also on their locations on the iceberg surface, the extended method estimates simultaneously the parameters in the iceberg motion model and the locations of the recorded sonar soundings in an iceberg-fixed reference frame.

The paper details the multi-objective least-squares estimation computation used in the iceberg motion and shape estimation. Included is a basis spline implementation for modeling and parameterizing the potentially complex iceberg trajectory. The paper presents results from simulated data to support the explanation of the method and demonstrate that the iceberg shape it recovers is less warped (relative to truth) than that generated under the assumptions used in previous work.

This work was supported by grant ANT-0811399 from the National Science Foundation.

I. Introduction

The use of Autonomous Underwater Vehicles (AUVs) for the study of free-floating icebergs is currently limited by the ability of AUVs to navigate accurately and safely with respect to such icebergs. Standard AUV navigation methods rely on inertial sensors and without inertial measurements of iceberg motion, they are unable to provide iceberg-relative vehicle position estimates. These estimates are necessary to enable an AUV to locate both itself and the scientific data it collects in an iceberg-centric reference frame. One way to obtain iceberg-relative AUV navigation estimates is to create a three-dimensional map of the iceberg's submerged surface and then use map-correlation of iceberg-pinging multibeam sonar range data to localize the vehicle within the map [1], [2].

The key challenge in creating a map of a free-floating iceberg is accounting for its motion through inertial space. Specifically, multibeam sonar soundings of an iceberg's submerged surface are necessarily expressed relative to the mapping vehicle and cannot be aggregated into an iceberg map unless the vehicle trajectory is known with respect to the iceberg. Because traditionally-available vehicle navigation instruments only provide measurements of vehicle trajectory in inertial space, they must be combined with an estimate of the iceberg's trajectory in inertial space in order to obtain the iceberg-relative vehicle trajectory required for mapping.

The mapping method presented in [1] accounts for iceberg motion by assuming that iceberg translation and rotation occur at rates which are constant throughout the duration of data collection. The values of these rates are chosen to maximize agreement between two small overlapping regions of multibeam sonar soundings from the beginning and end of a circumnavigation (loop closure). Given that the area of sonar overlap is small compared to total mapped area, loop closure only gives information about the total iceberg translation and rotation. While loop closure does enable creation of a self-consistent map, it does not provide any information about variation of the rates over the duration of data collection.

The constant velocity assumption can be inaccurate and an inaccurate model of iceberg motion results in some warping of the resulting iceberg map (with respect to the true shape of the iceberg). A more accurate iceberg motion model

could yield reduction in this warping. Although a warped but self-consistent map may be used successfully for vehicle localization as demonstrated in [2], reducing map warping will improve slightly the localization performance (accuracy, convergence rate, and required computation), and the scientific value of the map itself.

The extended iceberg mapping method presented in this paper utilizes an iceberg motion model which is more complex than the constant-velocity model used in previous work and as a result achieves an iceberg map which is less warped. To identify the parameters in this model, the extended method requires information in addition to what is available from loop closure based on small overlapping regions of multibeam data. It requires information about how the iceberg is moving throughout the entirety of the circumnavigation. This information can be obtained from measurements of iceberg-relative vehicle velocity made by a Doppler Velocity Logger (DVL).

Parameter values of the complex motion model are chosen both to satisfy loop closure and minimize the difference between iceberg velocities as predicted by the model and as measured by the DVL-equipped vehicle. Vehicle inertial navigation measurements are combined with DVL range and velocity measurements to give a measurement of the inertial-space position and velocity of each point on the iceberg surface ensonified by the DVL. The method exploits the explicit dependence of these measurements upon the trajectory and shape of the iceberg in order to estimate simultaneously (1) the parameters in the complex iceberg motion model and (2) the locations of DVL soundings within an iceberg-fixed reference frame.

This paper details the extended post-processing method. It presents a basis spline iceberg motion model, capable of representing complex trajectories. It shows the explicit dependencies of each measurement upon the parameters to be estimated, and formulates a multi-objective linear least-squares computation which minimizes the difference between measured and modeled quantities. Finally, the paper presents results from simulated data to support the explanation of the extended method and to demonstrate that the iceberg shape it recovers is less warped than that generated under assumptions as in [1].

II. Background

A. AUVs Under Ice

Numerous research programs have demonstrated that AUVs can operate successfully in the under-ice environment [3], [4], [5], [6], [7], [8], [9]. These programs have addressed important under-ice challenges such as vehicle deployment and recovery through ice, the inability of AUVs to obtain GPS navigation fixes while beneath ice, the reduced performance of navigation instruments at high-latitudes, and the hazardous presence of both ice and seafloor obstacles. In all of these deployments, AUVs have operated beneath ice fixed in inertial space (e.g. fast ice or ice shelves), and have used navigation inertially-referenced navigation techniques not designed to provide vehicle localization with respect to icebergs which are translating and rotating through inertial space.

The motivation for creating self-consistent maps of moving icebergs is that they can be used to provide iceberg-relative AUV navigation estimates.

B. Underwater Mapping Techniques

For seafloor mapping applications, terrain maps are created by casting sonar range-to-seafloor vectors recorded by a mapping vehicle from a best estimate of the vehicle trajectory along which they were collected. The sonar data used to create these maps can be collected from ship hull-mounted systems or from submerged vehicles such as towfish, ROVs and AUVs. The advantage of the submerged vehicles is that they can produce data of higher resolution due to their proximity to the seafloor. In either case, generating the map requires an accurate estimate of the vehicle's trajectory with respect to the terrain being mapped. For ship-based systems, this is relatively straightforward since the location of the ship relative to the seafloor is measurable using GPS. For submerged vehicle systems, a best estimate of the vehicle trajectory must be formed in other ways.

There are two common techniques for estimating an underwater vehicle's trajectory during mapping operations. One is to use acoustic arrays during data collection [10], [11]. The other is to exploit self-intersecting trajectories, and use terrain correlation at these intersection points to perform adjustments to the estimated vehicle trajectory in post-processing [12], [13].

The advantage of the self-intersecting trajectory technique is that it does not require the potentially problematic deployment and calibration of an acoustic array. In the iceberg application, this technique is complicated further by the requirement that the array be fixed to the iceberg. Note that acoustic arrays were successfully fixed to rather small icebergs (up to 100 m draft) for mapping in the Dynamics of Iceberg Grounding and Scouring (DIGS) experiment, but that their deployment was challenging even in calm conditions, and several operational problems with the method were identified [14].

The disadvantage of the self-intersecting trajectory technique is that the trajectory estimate it generates can be less accurate than acoustic array-based approaches since it lacks the continuous, direct measurement of vehicle position. Even so, the maps generated with this approach typically provide meter-level accuracy. Hence, the technique is in common use. In addition, software tools such as MB-System [15] exist which facilitate both the processing of the sonar data and the generation of best estimates of vehicle trajectory.

In order to generate maps of free-floating icebergs, the process of estimating the vehicles's trajectory during data collection must compensate for the motion of the iceberg. The method in [1] and the extended method presented here use iceberg surface shape correlation at the beginning and end of a circumnavigation in a manner similar to existing seafloor mapping techniques - to determine the trajectory of the mapping vehicle relative to the surface being mapped.

C. Basis Splines

This method utilizes basis splines to model and account for the motion of the iceberg during mapping. The basis spline is

a well-understood tool for fitting smooth curves to large data sets. Basis splines are a specific form of piecewise polynomial whose number of piecewise elements, polynomial degree, and continuity may be specified. Linear combinations of specified basis functions make up a basis spline. Evaluation of a basis spline is achieved simply through matrix multiplication of its basis functions by its control points. At any time for which the spline is defined, the value of the spline depends only upon a subset of the control points. Transition times between "active" basis functions are called knots. For more information on basis splines, including the specific forms of their constituent basis functions, see [16] and [17].

In the iceberg mapping method presented here, basis splines provide a general model of iceberg motion, whose parameters are identified using measurements of iceberg velocity.

D. The Doppler Velocity Logger

The DVL instrument provides measurements of vehicle-relative iceberg velocity and range which are required by the iceberg mapping method presented here. DVLs typically use four acoustic beams, each from a separate transducer, each pointed in a known direction (e.g. forming a square pyramid). DVLs used for navigation are configured to record both the travel time and Doppler shift (change in frequency) of the return echo from the seafloor or other surface in each beam direction. The echo travel time is multiplied by the local speed of sound to give range-to-surface for each beam, while the Doppler shift is used to recover the component of surface-relative velocity lying parallel to each beam. Under known geometry, the four beams provide overdetermined sets of range and velocity measurements from which a surface plane may be fit and the total surface-relative velocity of the instrument may be recovered. Often, a single range vector (in the center of the beam formation) to the fit surface plane is taken to be the distance of the vehicle from the surface (e.g. altitude for downward-looking DVLs).

Together with vehicle attitude data, DVL velocity measurements are numerically integrated to provide vehicle displacement estimates. Typically, DVLs provide measurements approximately five times per second, a rate which is fast compared to accelerations undergone by typical AUVs. Integration of seafloor-relative DVL velocity measurements is at the heart of a large number of currently fielded underwater vehicle navigation systems. DVLs have also been used to obtain vehicle velocity measurements for navigation with respect to ship hulls [18], and notably, with respect to sea ice [19] and ice shelves [6] fixed in inertial space.

The present method uses a DVL pointed at the submerged surface of an iceberg to obtain the single range ("altitude") to the iceberg surface, the velocity of the iceberg surface with respect to the vehicle, and the vehicle displacement (integrated velocity) with respect to the ice.

III. Data Collection

Map creation in this method is accomplished in post-processing. Three data sets comprise the required input for map creation, and must be collected by the AUV during circumnavigation of the iceberg:

1) **AUV Trajectory:** This data set includes both position and orientation of the mapping vehicle over time. It is defined in inertial space and is measured by standard means (e.g. vehicle inertial navigation system (INS), corrected by GPS fixes at deployment and recovery).
2) **DVL Soundings:** The DVL is pointed at the ice surface from the mapping vehicle and each ping yields two important measurements: a range vector from the vehicle to a point on the iceberg surface, and the vehicle-relative velocity of that point on the iceberg. The velocity may be integrated to obtain relative displacement. Necessarily, all DVL measurements are defined in the vehicle frame.
3) **Multibeam Sonar Pings:** Each ping yields a fan-shaped pattern of many (e.g. hundreds, depending on the model) range measurements from the vehicle to the iceberg surface. These range vectors are defined in the vehicle frame and lie in the across-track (standard vehicle YZ) plane.

Symbols representing these data are defined in Table I.

IV. Post-Processing

A. Approach

The mapping method works by choosing parameters in an iceberg motion model which best explain the collected data. The motion model is expressed here using splines for two reasons. First, by specifying the spline degree and number of knots, the complexity of the iceberg motion may be constrained in a physically reasonable way. Second, the spline representation is linear and facilitates a linear least-squares estimation method.

It is shown below that the collected inertial-space DVL sounding locations, inertial-space DVL velocities, and iceberg-frame sounding-to-sounding distances depend linearly on the control point locations of an iceberg position spline and linearly upon the iceberg-frame locations of the DVL soundings, but non-linearly upon the orientation of the iceberg. Because these three quantities are readily computed from vehicle data, the strategy employed is to feed "known" iceberg heading splines to a fast inner loop which selects iceberg position spline control points and iceberg-frame sounding locations via multi-objective linear least-squares to best fit the recorded data. This best fit depends on the heading spline used, so the outer loop uses least-squares residuals from the inner loop to search the control point space for the best heading spline.

Specifically, the multi-objective linear least-squares estimator used in this method works to minimize the weighted sum, J, of five objectives as in Equation 1.

$$J = \left\| A_1\vec{x} - {}^{I}\hat{\vec{x}} \right\|^2 + \mu_2 \left\| A_2\vec{x} - {}^{I}\hat{\dot{\vec{x}}} \right\|^2 + \mu_3 \left\| A_3\vec{x} - {}^{b}\hat{d} \right\|^2 + \mu_4 \left\| A_4\vec{x} \right\|^2 + \mu_5 \left\| A_5\vec{x} \right\|^2 \quad (1)$$

Here, $\hat{x}$ is the estimata vector, and contains the control points of the iceberg position spline as well as the iceberg-frame position of each point on the iceberg surface ensonified by

Measured Quantity	True Value	Instrument	Measurement
Time of i^{th} measurement	t_i	Clock	-
Vehicle position in inertial space	${}^{I}\vec{x}_v$	INS	${}^{I}\hat{x}_v$
Range vector from vehicle to i^{th} point on iceberg surface	${}^{v}\vec{r}_i$	DVL	${}^{v}\hat{\vec{r}}_i$
Vehicle-relative velocity of i^{th} point on iceberg surface	${}^{v}\dot{\vec{r}}_i$	DVL	${}^{v}\hat{\dot{\vec{r}}}_i$
Rotation Matrix from vehicle frame to inertial frame	${}^{I/v}R$	Compass/INS	${}^{I/v}\hat{R}$

TABLE I
MEASURED QUANTITIES AND SYMBOLS

the mapping vehicle's DVL. Each of the first four norms in Equation 1 is an indicator of how well the estimated iceberg trajectory and shape support the recorded data. Each $A_1 \dots A_4$ is a matrix which multiples the estimata vector to give the modeled value of a measured quantity. A_1 is the measurement model which multiplies $\hat{x}$ to give the inertial-space position of each point ensonified by the DVL, while measured values are contained in ${}^{I}\hat{\vec{x}}$. The matrix A_2 is the measurement model which multiplies $\hat{x}$, to give the modeled inertial-space velocity of each point ensonified by the DVL. Measured inertial-space velocities appear in the vector ${}^{I}\hat{\dot{\vec{x}}}$). The matrix A_3 multiplies $\hat{x}$ to give the modeled iceberg-frame distances between subsequent points ensonified by the DVL. Measurements of the sounding-to-sounding distances appear in ${}^{b}\hat{d}$. The matrix A_4 multiplies $\hat{x}$ to give the separation distance between twice-ensonified points (from the beginning and end of the circumnavigation) on the iceberg surface. Minimizing the norm of this product works to enforce loop-closure. Finally, A_5 multiplies $\vec{x}$ to give the vector sum of all the estimated iceberg-frame sounding locations. The location (on the iceberg) of the origin of the iceberg-fixed reference frame is arbitrary, so with a very small weight, μ_5, minimization of $\mu_5 \left\|A_5\vec{x}\right\|^2$ is used to pull the center of the reference frame toward the geometric center of the iceberg to prevent numerical issues.

The remainder of this section details the splines used to represent iceberg trajectory as well as the data sources and linear models $(A_1, \dots, A_5)$ used in the least-squares solution.

B. Spline Representation of Iceberg Trajectory

In this method, basis splines are used to represent iceberg motion, and choices in spline configuration have important physical meanings. For example, increasing the number of piecewise elements allows for a higher temporal frequency in the trajectory represented by the spline. Also, the degree of the polynomial used may be interpreted as a limitation on the acceleration of (and therefore force or torque acting upon) the iceberg. For example, a continuous second order piecewise polynomial representing position also represents through its derivatives a piecewise constant, generally discontinuous acceleration or force history. Similarly, a continuous third order piecewise position polynomial corresponds to a piecewise linear, continuous acceleration or force history.

Ideally, to minimize the number of parameters to be estimated, the number of piecewise elements and the polynomial degree used should each be as small as possible while maintaining the ability to describe accurately the motion of the iceberg. In practice, because the motion of the iceberg is unknown, the values used must depend on the size of the iceberg being mapped, the duration of the circumnavigation, and possibly also on observations of local weather conditions and ocean currents.

Spline representations of inertial-space position and orientation of the iceberg-fixed reference frame used here are given in Equations 2 and 3.

$$ {}^{I}\hat{\vec{x}}_b(t) = B_{1,D_x}(t)I\vec{P}_{x,1} + B_{2,D_x}(t)I\vec{P}_{x,2} + \dots + B_{n,D_x}(t)I\vec{P}_{x,N_x} \quad (2) $$

$$ {}^{I}\hat{\psi}_b(t) = B_{1,D_\psi}(t)P_{\psi,1} + B_{2,D_\psi}(t)P_{\psi,2} + \dots + B_{n,D_\psi}(t)P_{\psi,N_\psi} \quad (3) $$

Here, D_x and D_ψ are the degree of the position and heading splines, respectively. N_x and N_ψ are the number of control points in the two splines. Note that the position spline is vector-valued, while the heading spline is scalar-valued.

Under the approach used here, it is important that the position of the iceberg frame may be described as a linear function of its control points. Specifically, at the time of the i^{th} measurement, the iceberg-frame position and translation rate are given by the matrix multiplications in Equations 4 and 5 (quantities appear beneath a hat when they are measured or estimated). Importantly, the position spline differs from the translation rate spline only in its basis functions (B vs $\dot{B}$), not in its control points.

$$ \begin{aligned} &{}^{I}\hat{\vec{x}}_b(t_i) \\ &= \begin{bmatrix} B_{1,D_x}(t_i)I & B_{2,D_x}(t_i)I & \dots & B_{N_x,D_x}(t_i)I \end{bmatrix} \vec{P}_x \\ &= B_x(t_i)\vec{P}_x \end{aligned} \quad (4) $$

$$ \begin{aligned} &{}^{I}\hat{\dot{\vec{x}}}_b(t_i) \\ &= \begin{bmatrix} \dot{B}_{1,D_x}(t_i)I & \dot{B}_{2,D_x}(t_i)I & \dots & \dot{B}_{N_x,D_x}(t_i)I \end{bmatrix} \vec{P}_x \\ &= \dot{B}_x(t_i)\vec{P}_x \end{aligned} \quad (5) $$

Here, $\vec{P}_x$ is a stacked vector containing the N_x control points for the position spline. The basis functions depend on the degree of the spline being used, and on the number of knots being used.

C. Inertial-Space Iceberg Surface Locations

The i^{th} DVL sounding yields a measured range vector to a point on the iceberg surface. The i^{th} such measurement is

denoted ${}^{v}\hat{\vec{r}}_i$. Combined with a measurement of vehicle position in inertial space at the time of the i^{th} measurement, ${}^{I}\hat{\vec{x}}_v(t_i)$, and a measurement of the rotation matrix from the vehicle frame to inertial space, ${}^{I/v}\hat{R}(t_i)$, this measurement gives the position in inertial space at time t_i of the i^{th} point on the iceberg surface as in Equation 6.

$$ {}^{I}\hat{\vec{x}}_i(t_i) = {}^{I}\hat{\vec{x}}_v(t_i) + {}^{I/v}\hat{R}(t_i){}^{v}\hat{\vec{r}}_i \tag{6} $$

The inertial-space position of this point on the iceberg is also expressed in terms of its position in the iceberg reference frame, ${}^{b}\vec{x}_i$, the position of the iceberg frame in inertial space at the time of the measurement, ${}^{I}\vec{x}_b(t_i)$, and a rotation matrix from the iceberg frame to inertial space at the time of the measurement, ${}^{I/b}R(t_i)$. Using the spline-derived estimates for these quantities, the modeled inertial-space position of the i^{th} point on the iceberg surface is computed as in Equation 7.

$$ {}^{I}\hat{\vec{x}}_i(t_i) = {}^{I}\hat{\vec{x}}_b(t_i) + {}^{I/b}\hat{R}(t_i){}^{b}\hat{\vec{x}}_i \tag{7} $$

The least-squares formulation works to minimize the difference between the measured and modeled values (Equations 6 and 7, respectively) of inertial-space position for all measurements, $i = 1, 2, \ldots, n$.

D. Inertial-Space Iceberg Surface Velocities

Combined with information from the vehicle inertial navigation system, the i^{th} DVL sounding yields a measurement of the velocity of the i^{th} point on the iceberg surface through inertial space, ${}^{I}\hat{\dot{\vec{x}}}_i$, as in Equation 8.

$$ {}^{I}\hat{\dot{\vec{x}}}_i = {}^{I}\hat{\dot{\vec{x}}}_v(t_i) + {}^{I/v}\hat{R}(t_i){}^{v}\hat{\dot{\vec{r}}}_i \tag{8} $$

Here, ${}^{I}\hat{\dot{\vec{x}}}_v(t_i)$ is the measured vehicle velocity in inertial space, ${}^{I/v}\hat{R}(t_i)$ is the rotation matrix from the vehicle frame to inertial space, and ${}^{v}\hat{\dot{\vec{r}}}_i$ is the DVL-measured vehicle velocity with respect to the ice, all at the time of the i^{th} DVL sounding.

Equation 9 gives the modeled inertial-space velocity of the i^{th} point on the iceberg surface.

$$ {}^{I}\hat{\dot{\vec{x}}}_i = {}^{I}\hat{\dot{\vec{x}}}_b(t_i) + {}^{I/b}\hat{R}(t_i)({}^{b}\hat{\vec{\omega}}_b(t_i) \times {}^{b}\hat{\vec{x}}_i) \tag{9} $$

Here, ${}^{I}\hat{\dot{\vec{x}}}_b(t_i)$ is the inertial-space velocity of the origin of the iceberg frame, given by the spline position estimate. ${}^{I/b}\hat{R}(t_i)$, the rotation matrix from the iceberg frame to inertial space, and ${}^{b}\hat{\vec{\omega}}_b$, the rotation rate of the iceberg, are each given by the spline heading estimate. Again, ${}^{b}\hat{\vec{x}}_i$ is the position in the iceberg frame of the i^{th} ensonified point on the iceberg surface.

The least-squares formulation works to minimize the difference between the measured and modeled values of the inertial-space surface velocities (Equations 8 and 9, respectively).

E. Iceberg-Frame Sounding-to-Sounding Distances

The $i = 1, 2, \ldots, n$ soundings used in this method represent only a sparse selection of the DVL soundings made over the course of data collection because consideration of every DVL sounding could render the estimation problem intractable. (Typical DVL instruments ping at a rate of approximately 5 Hz).

Instead of including explicitly the velocity measurement from every DVL sounding, the method includes measurements of iceberg-relative vehicle displacement between selected soundings, obtained by integration of the DVL velocity signal.

The derived measurement of the iceberg-frame displacement vector between the i^{th} selected point on the iceberg surface and the selected point preceding it is given by ${}^{b}\hat{\vec{d}}_i$. It is defined in terms of measured quantities in Equation 10.

$$ {}^{b}\hat{\vec{d}}_i = {}^{b/v}\hat{R}(t_{i-1})({}^{v}\hat{\vec{d}}_v(t_i) - {}^{v}\hat{\vec{r}}_{i-1}) + {}^{b/v}\hat{R}(t_i){}^{v}\hat{\vec{r}}_i \tag{10} $$

Here, ${}^{b/v}\hat{R}(t_{i-1})$ and ${}^{b/v}\hat{R}(t_i)$ are the rotation matrices from the vehicle frame to the iceberg frame at time (t_{i-1}) and (t_{i-1}), respectively. These rotation matrices are derived both from the measured vehicle attitude and the estimated iceberg orientation. The vector, ${}^{v}\hat{\vec{d}}_v(t_i)$ is the distance traveled by the vehicle relative to the iceberg between (t_{i-1}) and (t_i). It is computed by the DVL via integration of ice-relative velocity (at approximately 5 Hz). The range vectors measured by the DVL at (t_{i-1}) and (t_i) are ${}^{v}\hat{\vec{r}}_{i-1}$ and ${}^{v}\hat{\vec{r}}_i$, respectively.

The modeled iceberg-frame distance between selected soundings is simply the vector difference between them, as in Equation 11.

$$ {}^{b}\hat{\vec{d}}_i = {}^{b}\vec{x}_i - {}^{b}\vec{x}_{i-1} \tag{11} $$

The least-squares estimation minimizes the difference between measured and modeled values of the iceberg-frame distance between soundings. Note that because the measured values depend on iceberg heading, they must be recomputed (under the "known" heading) for each multi-objective least-squares estimation.

F. Loop Closure

Loop closure is the idea that the mapping vehicle ensonifies the same section of the iceberg surface at the beginning and end of its circumnavigation. If loop closure is properly enforced, the estimated iceberg-frame positions of points ensonified at the beginning and end of the iceberg circumnavigation are equal, even though the measured inertial-space positions of each such point may have been largely disparate.

Determination of sounding pairs representing the same point on the iceberg surface is performed by aligning the multibeam sonar data. This can be achieved with a simple constant velocity motion model as in [1], or by a point cloud alignment algorithm such as ICP [20]. Since the multibeam range vectors and DVL range vectors are each defined in the vehicle frame, alignment of the multibeam soundings yields alignment of the DVL soundings.

In the least-squares estimation, loop closure is achieved by minimizing the iceberg-frame difference between each pair of matched sounding locations. Note that rather than as one-to-one sounding matches, loop closure could also be described with linear combinations of sounding locations (e.g. a particular sounding from the end of the circumnavigation sits at some weighted average position of two adjacent soundings from the beginning of the circumnavigation).

G. Frame Centering

The location on the iceberg of the origin of the iceberg-fixed reference frame is arbitrary. For a given iceberg motion, the arrangement of sounding locations can be shifted anywhere in the reference frame so long as the trajectory of the frame origin is adjusted correspondingly.

The final objective in the least-squares minimization is one which pulls the origin of the iceberg frame toward the geometric center of the iceberg. Specifically, the objective to be minimized is the squared norm of the vector sum of all the iceberg-frame sounding locations. If an adequately complex model of iceberg motion is included (i.e. enough piecewise elements and high enough degree), a very small weighting of this objective is sufficient to center the reference frame on the iceberg without penalizing the other objectives.

H. Multiobjective Least-Squares Solution

Equating the measured and modeled values (detailed in these sectionsIV-C - IV-G) for all $i = 1, 2, \ldots, n$ DVL soundings gives an overdetermined system of equations, all of which are linear in the iceberg position spline control points and iceberg-frame locations of points ensonified by the mapping vehicle DVL. This system is written in matrix form in Equations 12 - 16. In each of these, the notation used in the original statement of the to-be-minimized cost function (Equation 1) is given on the left, while the expanded matrix form is given on the right.

There a total of $3n + r$ vector equations, and $n + N_x$ vector unknowns, where r is the number of redundantly-ensonified points on the iceberg surface. Values for the weights $\mu_2, \ldots, \mu_5$ should be determined based on the uncertainties of the sensors used in the relevant measurements. The estimate which minimizes the cost function in Equation 1 is $\hat{\vec{x}}_{ls}$, as given in Equation 17.

$$\hat{\vec{x}}_{ls} = \begin{bmatrix} A_1 \\ \sqrt{\mu_2}A_2 \\ \sqrt{\mu_3}A_3 \\ \sqrt{\mu_4}A_4 \\ \sqrt{\mu_5}A_5 \end{bmatrix}^{\dagger} \begin{bmatrix} {}^{I}\hat{\vec{x}} \\ \sqrt{\mu_2}\,{}^{I}\hat{\dot{\vec{x}}} \\ \sqrt{\mu_3}\,{}^{b}\hat{\vec{d}} \\ 0 \\ 0 \end{bmatrix} \tag{17}$$

Here, the superscripted † gives the pseudoinverse of the preceding matrix.

I. Outer Loop Heading Estimate

Recall that the linear models used in the least-squares estimate all rely on a "known" iceberg heading trajectory over the duration of the map data collection. An outer loop must function to supply these heading trajectories to the inner least-squares estimation. The outer loop chooses the best estimate of heading trajectory as the one which yields the least-squares residual (from the inner loop) of lowest norm squared. The form used by the outer loop to represent heading trajectory does not affect the workings of the inner loop. (Here, it has been formulated using a basis spline to represent heading). The least-squares residual, $\tilde{\vec{x}}$, is given in Equation 18.

$$\tilde{\vec{x}} = \begin{bmatrix} A_1 \\ \sqrt{\mu_2}A_2 \\ \sqrt{\mu_3}A_3 \\ \sqrt{\mu_4}A_4 \\ \sqrt{\mu_5}A_5 \end{bmatrix} \hat{\vec{x}}_{ls} - \begin{bmatrix} {}^{I}\hat{\vec{x}} \\ \sqrt{\mu_2}\,{}^{I}\hat{\dot{\vec{x}}} \\ \sqrt{\mu_3}\,{}^{b}\hat{\vec{d}} \\ 0 \\ 0 \end{bmatrix} \tag{18}$$

V. Results

Simulated planar data are used here to demonstrate the extended mapping method. The data include the (invented) true shape and non-inertial trajectory of an iceberg as well as simulated vehicle navigation and ice-pinging DVL velocity measurements from circumnavigation. In this example, the iceberg perimeter is 3.36 km and the iceberg area is 0.61 km^2. The mapping vehicle moves at 1.5 m/s and therefore takes approximately 38 minutes to circumnavigate the iceberg. Meanwhile, the iceberg moves non-inertially with slowly-varying translational velocities between 0.046 and 0.047 m/s and heading rates between 2.4 and 4.8 rad/s.

The simulated vehicle circumnavigation trajectory appears in Figure 1. Accumulated dead-reckoning error of approximately 3.5% of distance traveled is also simulated for the trajectory. This error is linearly backsmoothed based on inertial fixing (e.g. as could be performed using GPS at vehicle deployment and recovery). Magnitude of simulated error in vehicle trajectory before and after inertial fixing appears in Figure 2. Note also that measurements of iceberg-frame sounding-to-sounding distances in this simulation are corrupted by zero-mean Gaussian noise with standard deviation equal to 1% of distance traveled (1 cm for every 10 m traveled relative to the iceberg).

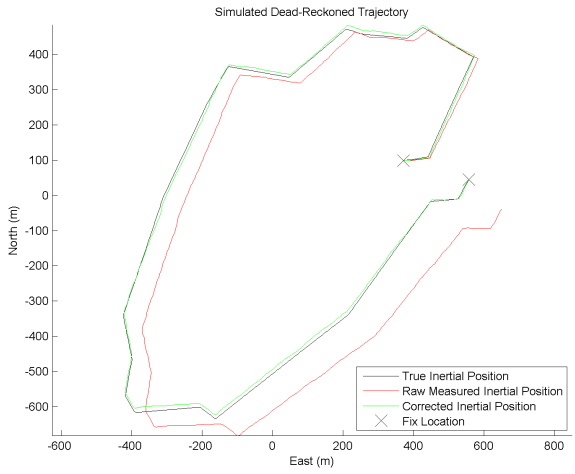

Fig. 1. Iceberg circumnavigation trajectory simulated with dead-reckoning error and inertial fixing

In this example, the outer loop is implemented using a four element (five knot) scalar-valued cubic spline to describe iceberg heading over time (see Equation 3). Selection of the heading spline control point values was achieved by a gradient-decent optimization, initialized with a vector zeros.

Inertial-space positions
${}^{I}\hat{\vec{x}} = A_1\vec{x}$
(n vector equations)

$$\begin{bmatrix} {}^{I}\hat{\vec{x}}_1(t_1) \\ {}^{I}\hat{\vec{x}}_2(t_2) \\ \vdots \\ {}^{I}\hat{\vec{x}}_n(t_n) \end{bmatrix} = \begin{bmatrix} B_x(t_1) & {}^{I/b}\hat{R}(t_1) & 0 & \dots & 0 \\ B_x(t_2) & 0 & {}^{I/b}\hat{R}(t_2) & \dots & 0 \\ \vdots & \vdots & \vdots & \ddots & \vdots \\ B_x(t_n) & 0 & 0 & \dots & {}^{I/b}\hat{R}(t_n) \end{bmatrix} \begin{bmatrix} \vec{P}_x \\ {}^{b}\vec{x}_1 \\ {}^{b}\vec{x}_2 \\ \vdots \\ {}^{b}\vec{x}_n \end{bmatrix} \tag{12}$$

Inertial-space velocities
${}^{I}\hat{\dot{\vec{x}}} = A_2\vec{x}$
(n vector equations)

$$\begin{bmatrix} {}^{I}\hat{\dot{\vec{x}}}_1(t_1) \\ {}^{I}\hat{\dot{\vec{x}}}_2(t_2) \\ \vdots \\ {}^{I}\hat{\dot{\vec{x}}}_n(t_n) \end{bmatrix} = \begin{bmatrix} \dot{B}_x(t_1) & {}^{I/b}\hat{R}(t_1)\hat{\Omega}(t_1) & 0 & \dots & 0 \\ \dot{B}_x(t_2) & 0 & {}^{I/b}\hat{R}(t_2)\hat{\Omega}(t_2) & \dots & 0 \\ \vdots & \vdots & \vdots & \ddots & \vdots \\ \dot{B}_x(t_n) & 0 & 0 & \dots & {}^{I/b}\hat{R}(t_n)\hat{\Omega}(t_n) \end{bmatrix} \begin{bmatrix} \vec{P}_x \\ {}^{b}\vec{x}_1 \\ {}^{b}\vec{x}_2 \\ \vdots \\ {}^{b}\vec{x}_n \end{bmatrix} \tag{13}$$

Sounding-to-sounding
${}^{b}\hat{d} = A_3\vec{x}$
($n-1$ vector equations)

$$\begin{bmatrix} {}^{b}\hat{\vec{d}}_2 \\ {}^{b}\hat{\vec{d}}_3 \\ \vdots \\ {}^{b}\hat{\vec{d}}_n \end{bmatrix} = \begin{bmatrix} 0 & -I & I & 0 & \dots & 0 \\ 0 & 0 & -I & I & \dots & 0 \\ \vdots & \vdots & \vdots & \ddots & \ddots & \vdots \\ 0 & 0 & 0 & \dots & -I & I \end{bmatrix} \begin{bmatrix} \vec{P}_x \\ {}^{b}\vec{x}_1 \\ {}^{b}\vec{x}_2 \\ \vdots \\ {}^{b}\vec{x}_n \end{bmatrix} \tag{14}$$

Loop closure
$0 = A_4\vec{x}$
(r vector equations)

$$\begin{bmatrix} 0 \\ 0 \\ \vdots \\ 0 \end{bmatrix} = \begin{bmatrix} 0 & I & 0 & \dots & -I & 0 & \dots & 0 \\ 0 & 0 & I & \dots & 0 & -I & \dots & 0 \\ \vdots & \vdots & \vdots & \ddots & \vdots & \vdots & \ddots & \vdots \\ 0 & 0 & 0 & \dots & 0 & 0 & \dots & -I \end{bmatrix} \begin{bmatrix} \vec{P}_x \\ {}^{b}\vec{x}_1 \\ {}^{b}\vec{x}_2 \\ \vdots \\ {}^{b}\vec{x}_n \end{bmatrix} \tag{15}$$

Frame centering
$0 = A_5\vec{x}$
(1 vector equation)

$$\begin{bmatrix} 0 \end{bmatrix} = \begin{bmatrix} 0 & I & I & I & \dots \end{bmatrix} \begin{bmatrix} \vec{P}_x \\ {}^{b}\vec{x}_1 \\ {}^{b}\vec{x}_2 \\ \vdots \\ {}^{b}\vec{x}_n \end{bmatrix} \tag{16}$$

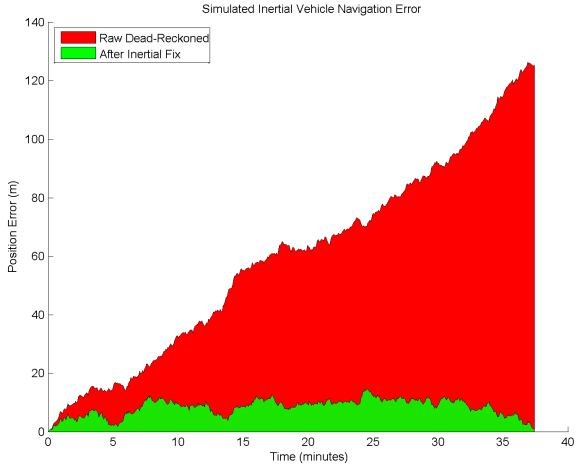

Fig. 2. Magnitude of simulated error in vehicle inertial navigation

Using the eventual best-estimate heading trajectory from the outer loop, Figures 3 and 4 show the inner loop least-squares fit of inertial-space iceberg surface position and velocity, respectively. Results shown here use a four element (five knot) vector-valued cubic spline to represent iceberg position. Multi-objective least-squares weightings are $\mu_2 = 5e^6$, $\mu_3 = 1e^5$, $\mu_4 = 1e^4$, and $\mu_5 = 1e^{-2}$.

The iceberg-frame sounding locations resulting from the estimation process appear along with the true iceberg shape and true sounding locations in Figure 5. The estimated shape is self-consistent, and the rms error of the estimated iceberg-frame sounding locations is 0.84 m.

Figure 6 shows the true and estimated sounding locations in the area of loop-closure. Note that both position estimates of each twice-ensonified point on the iceberg appear within 25 cm of each other, and that this distance depends on the choice of μ_4.

Finally, Figure 7 shows a detail view along one side of the iceberg, including positions estimated by the extended method presented in this paper and positions estimated under

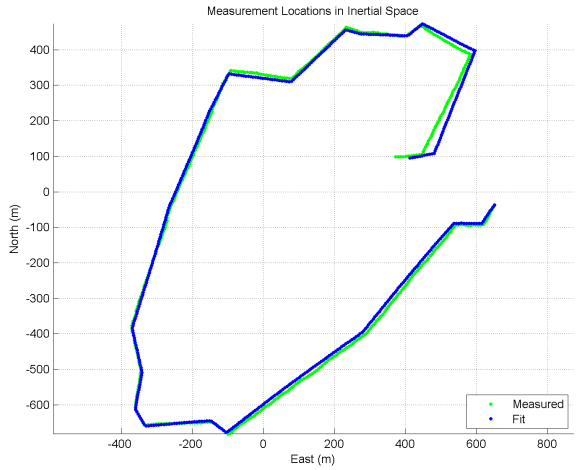

Fig. 3. Least-squares fit to the measured inertial-space locations of points on the iceberg surface

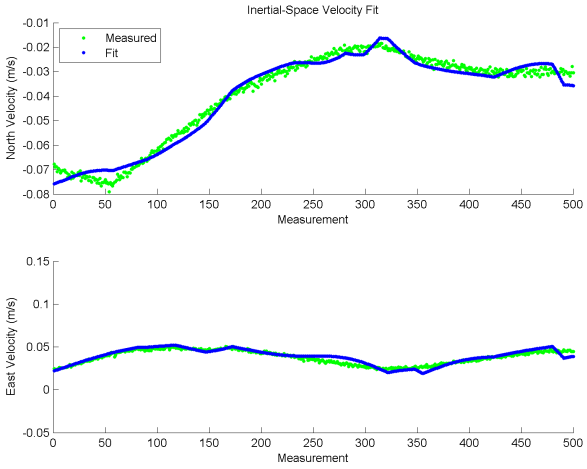

Fig. 4. Least-squares fit to the measured inertial-space velocities of points on the iceberg surface

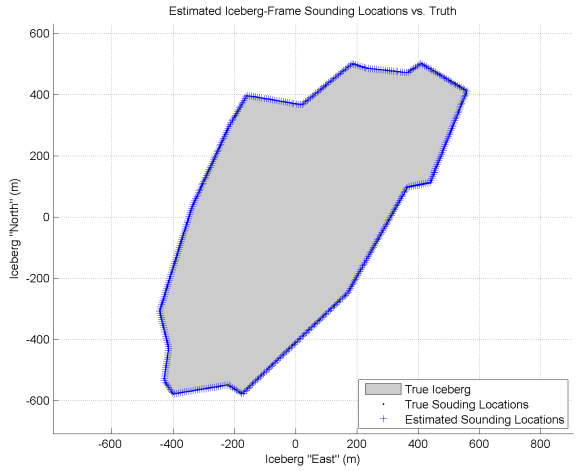

Fig. 5. Estimated positions in the iceberg frame of ensonified points on the iceberg surface (0.84 m rms error)

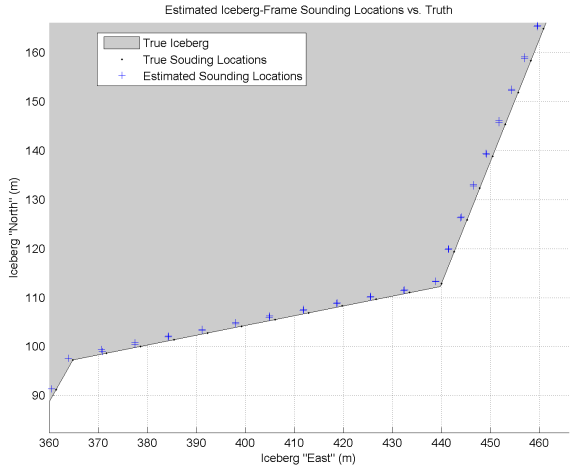

Fig. 6. Detail view at loop closure

assumptions equivalent to those in [1] (e.g. no velocity measurements and constant iceberg translation and rotation rates). Note that less warping is evident in the positions estimated by the extended method. Over the entire circumnavigation, the rms error between the estimated and true sounding locations is 0.84 m for the extended method and 4.83 m for the method as in previous work.

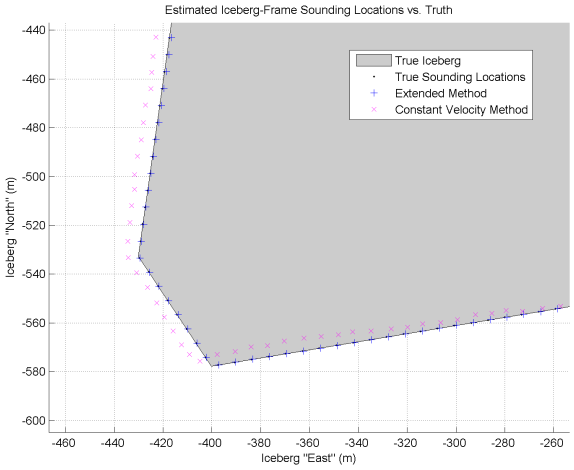

Fig. 7. Detail view comparing iceberg shape estimation results of the extended and original methods

VI. Conclusion

The post-processing iceberg mapping method presented here incorporates an iceberg motion model which is more general than the constant velocity model used in previous work. This model is capable of describing more accurately the trajectory of the iceberg through inertial space, and therefore yields an iceberg map whose shape is closer to the true shape of the iceberg. To identify the parameters in this model, the method includes Doppler Velocity Logger measurements of iceberg-relative mapping vehicle velocity, which are available over the entire duration of map data collection.

The mapping method works by modeling iceberg motion to minimize the difference between modeled and measured AUV sensor data. The method utilizes basis splines to model and constrain the space of possible iceberg trajectories. Measurements considered in this minimization include inertial-space position and velocity of points on the iceberg surface as well as the total physical separation between points on the iceberg surface. As in previous work, the extended method also relies upon loop closure, the fact that the AUV passes over the same section of the iceberg surface both at the beginning and end of its circumnavigation, to generate the best possible estimate.

Specifically, it is shown in Section IV that AUV measurements of inertial-space position and velocity of points on the iceberg surface (1) depend linearly upon the control points of a spline describing the position of the origin of the iceberg-fixed frame in inertial space; (2) depend linearly upon the positions of those points in a frame attached to the iceberg; and (3) depend non-linearly upon the heading of the iceberg. The estimation procedure is structured as an outer loop over iceberg heading surrounding and a fast linear least-squares estimator of iceberg position spline control points and iceberg-frame sounding locations.

A sample result based on simulated data demonstrates recovery of a self-consistent iceberg map with 0.84 m rms error in the estimated locations of soundings within a reference frame attached to the iceberg. With actual mapping data including multibeam sonar, the iceberg trajectory estimate recovered would be used to aggregate the multibeam soundings in the iceberg-fixed reference frame, yielding a self-consistent three-dimensional map suitable for iceberg-relative vehicle navigation.

REFERENCES

[1] Peter Kimball and Stephen Rock, "Sonar-Based Iceberg-Relative AUV Navigation", in *Proceedings Of AUV2008*, Woods Hole, MA, October 2008, IEEE.

[2] Peter Kimball and Stephen Rock, "Sonar-Based Iceberg-Relative AUV Localization", in *UUST: Unmanned Untethered Submersible Technology*, Richard Blidberg, Ed., Durham, NH, August 2009, Autonomous Undersea Systems Institute.

[3] J.G. Bellingham, C.A. Goudey, T.R. Consi, J.W. Bales, D.K. Atwood, J.J. Leonard, and C. Chryssostomidis, "A second generation survey auv", in *Symposium on Autonomous Underwater Vehicle Technology*. AUV Technology, July 1994, pp. 148–155.

[4] Bruce Butler and Ron Verrall, "A precision hybrid inertial/acoustic navigation system for a long-range autonomous underwater vehicle", in *AM 98*. Institute of Navigation, 1998, pp. 561–572.

[5] Rob McEwen, Hans Thomas, Don Weber, and Frank Psota, "Performance of an auv navigation system at arctic latitudes", *IEEE Journal of Oceanic Engineering*, vol. 30, no. 2, pp. 443–454, April 2005.

[6] K. W. Nicholls, E. P. Abrahamsen, J. J. H. Buck, P. A. Dodd, C. Goldblatt, G. Griffiths, K. J. Heywood, N. E. Hughes, A. Kaletzky, G. F. Lane-Serff, S. D. McPhail, N. W. Millard, K. I. C. Oliver, J. Perrett, M. R. Price, C. J. Pudsey, K. Saw, K. Stansfield, M. J. Stott, P. Wadhams, A. T. Webb, and J. P. Wilkinson, "Measurements beneath an antarctic ice shelf using an autonomous underwater vehicle", *Geophysical Research Letters*, vol. 33, April 2006.

[7] P. Wadhams and MJ Doble, "Digital terrain mapping of the underside of sea ice from a small AUV", *Geophysical Research Letters*, vol. 35, no. 1, 2008.

[8] Clayton Kunz, Chris Murphy, Hanumant Singh, Claire Pontbriand, Robert A. Sohn, Sandipa Singh, Taichi Sato, Christopher N. Roman, Ko ichi Nakamura, Michael V. Jakuba, Ryan Eustice, Richard Camilli, and John Bailey, "Toward extraplanetary under-ice exploration: Robotic steps in the arctic.", *Journal of Field Robotics*, vol. 26, no. 4, pp. 411–429, 2009.

[9] Kristof Richmond, Shilpa Gulati, Christopher Flesher, Bartholomew Hogan, and William Stone, "Navigation, Control, and Recovery of the Endurance Under-Ice Hovering AUV", in *UUST: Unmanned Untethered Submersible Technology*, Richard Blidberg, Ed., Durham, NH, August 2009, Autonomous Undersea Systems Institute.

[10] Vicki Lynn Ferrini, Daniel J. Fornari, Timothy M. Shank, James C. Kinsey, Maurice A. Tivey, S. Adam Soule, Suzanne M. Carbotte, Louis L. Whitcomb, Dana Yoerger, and Jonathan Howland, "Submeter bathymetric mapping of volcanic and hydrothermal features on the East Pacific Rise crest at 950degN", *Geochemistry, Geophysics, and Geosystems*, vol. 8, no. 1, January 2007.

[11] Dana R. Yoerger, Michael Jakuba, and Albert M. Bradley, "Techniques for deep sea near bottom survey using an autonomous underwater vehicle", *International Journal of Robotics Research*, vol. 26, no. 1, pp. 41–54, January 2007.

[12] WJ Kirkwood, "Development of the DORADO mapping vehicle for multibeam, subbottom, and sidescan science missions: Research Articles", *Journal of Field Robotics*, vol. 24, no. 6, pp. 487–495, 2007.

[13] Chris Roman and Hanumant Singh, "Improved vehicle based multibeam bathymetry using sub-maps and slam", in *Intelligent Robots and Systems*. IEEE/RSJ International, Aug 2005, pp. 3662– 3669.

[14] Canadian Seabed Research Limited, "Techniques for determining the maximum draft of an iceberg", *Canadian Hydrography Centre Report*, , no. 20-46, 2000.

[15] "MB-System Software Package, http://www.mbari.org/data/mbsystem/html/mbsystem_home.html".

[16] Carl de Boor, *A Practical Guide to Splines*, Springer-Verlag Berlin and Heidelberg GmbH & Co. K, 1978.

[17] Les A. Piegl and Wayne Tiller, *The Nurbs Book*, Springer, 1997.

[18] J. Vaganay, M.L. Elkins, S. Willcox, F.S. Hover, R.S. Damus, S. Desset, J.P. Morash, and V.C. Polidoro, "Ship hull inspection by hull-relative navigation and control", in *OCEANS, 2005. Proceedings of MTS/IEEE*, 2005, pp. 761 – 766 Vol. 1.

[19] P. Wadhams, J. P. Wilkinson, and A. Kaletzky, "Sidescan sonar imagery of the winter marginal ice zone obtained from an auv", *AMS Journal of Atmospheric and Oceanic Technology*, vol. 21, pp. 1462–1470, 2004.

[20] P.J. Besl and N.D. McKay, "A Method for Registration of 3-D Shapes", *IEEE Transactions on Pattern Analysis and Machine Intelligence*, vol. 14, no. 2, pp. 239–256, 1992.